MULTIDIMENSIONAL CHARACTERIZATION OF THERMALLY ACTUATED SHAPE MEMORY POLYMER NEUROVASCULAR STENTS

A Senior Scholars Thesis

by

LANDON D. NASH

Submitted to Honors and Undergraduate Research
Texas A&M University
in partial fulfillment of the requirements for the designation as

UNDERGRADUATE RESEARCH SCHOLAR

May 2012

Major: Biomedical Engineering

MULTIDIMENSIONAL CHARACTERIZATION OF THERMALLY ACTUATED SHAPE MEMORY POLYMER NEUROVASCULAR STENTS

A Senior Scholars Thesis

by

LANDON D. NASH

Submitted to Honors and Undergraduate Research
Texas A&M University
in partial fulfillment of the requirements for the designation as

UNDERGRADUATE RESEARCH SCHOLAR

Approved by:

Research Advisor: Duncan J. Maitland
Associate Director, Honors and Undergraduate Research: Duncan MacKenzie

May 2012

Major: Biomedical Engineering

ABSTRACT

Multidimensional Characterization of Thermally Actuated Shape Memory Polymer Neurovascular Stents. (May 2012)

Landon D. Nash
Department of Biomedical Engineering
Texas A&M University

Research Advisor: Dr. Duncan J. Maitland
Department of Biomedical Engineering

In this work, shape memory polymer neurovascular stent prototypes based on a previously proposed design were thermo-mechanically characterized to expand on the clinical efficacy of the device. The stents were made by dip-coating pins in a thermoplastic polymer solution and subsequently covalently crosslinking the polymer using UV irradiation to yield thermoset tubes. These crosslinked tubes were CO_2 laser engraved to produce the complex stent geometry.

Experiments were conducted to determine the physiologically relevant mechanical behavior of these devices. Three point bend tests were performed to determine the longitudinal flexibility of deployed stents at room temperature and body temperature. The resulting longitudinal flexibility data was compared to currently available stent systems. Radial behavior tests were conducted on stent prototypes and polymer tubes using a radial compression system that interfaces with a tensile tester. Crimping and radial recovery behavior experiments measured the pressure exerted by the device as a

function of strain recovery at discrete temperatures. Crimped polymer tubes, representing idealized polymer stents, were deployed in the compression station at fixed diameters. These tests represented the constrained recovery environment of an occluded vessel and quantified recovery pressures as a function of temperature. Material characterization techniques such as dynamic mechanical analysis, tensile testing, and gel fraction studies were employed to further quantify the clinical relevance of this device.

These devices proved to have longitudinal flexibility values comparable to or better than many stents currently available on the market, which makes them attractive for neurovascular applications requiring navigation of tortuous vessels. Additionally, shape memory tests demonstrated a one second device deployment, which minimizes the amount of heat introduced into the body. This study also provides a body of data useful for further optimization of this medical device, such as desirable crimping pressures, optimal crimping temperatures, and device deployment pressures.

DEDICATION

I dedicate this thesis to my mother. She is the foundation of my amazing family, and I love her dearly.

ACKNOWLEDGMENTS

This thesis would not have been possible without the help, insight, and advice of several people that I respect very highly.

I'd like to thank Dr. Duncan Maitland for the opportunity to work in his lab. His advice and the experience that I have gained working for him have been the most valuable aspects of my undergraduate career. He is an exceptional advisor.

Thanks to my mentor Brent Volk for his guidance and advice throughout the course of this project. He is one of the most genuinely nice, humble, but brilliant people I've had the pleasure of meeting.

Thanks to Keith Hearon for teaching me how to conduct research, properly make sweet tea, showing me the ins and outs of plastic, clarifying that Texas is definitely not part of the South, and most of all for giving sound life advice that comes from experience. You're a great friend.

I would have no molecular weight data if it weren't for the help of Alex Lonnecker from Dr. Karen Wooley's group in the Chemistry Department at Texas A&M. Thank you for making the method and running my samples.

Finally I would like to thank my loving family for their infinite support, particularly my parents. You've all set a great example for me.

NOMENCLATURE

2-but	2-butene-1,4-diol
AA	Allyl Alcohol
DMA	Dynamic Mechanical Analysis
DMPA	2,2-Dimethoxy-2-phenyl-acetophenone
FDA	Food and Drug Administration
PSI	Pounds Per Square Inch
PU	Polyurethane
SEC	Size Exclusion Chromatography
SMP	Shape Memory Polymer
T_g	Glass Transition Temperature
THF	Tetrahydrofuran
TRF	Total Radial Force
TMHDI	Trimethylhexamethylene diisocyanate
UV	Ultraviolet

TABLE OF CONTENTS

Page

LIST OF FIGURES

FIGURE Page

LIST OF TABLES

CHAPTER I

INTRODUCTION

The focus of this work is to characterize the thermo-mechanical behavior of thermally actuated, amorphous, covalently crosslinked shape memory polymers (SMPs), which recover from a temporary shape to a primary shape when heat is applied. This shape memory property makes these materials attractive for a wide variety of biomedical applications[1-3], including minimally invasive endovascular interventions[4-7].

Clinical motivation

In the United States, a person has a stroke approximately every 40 seconds[8]. Current stroke intervention procedures such as aneurysm coiling and carotid artery stenting display clinical success in treating stroke, but there is still a need for better therapies. There is a particularly large clinical gap in the treatment of ischemic stroke due to intracranial atherosclerosis[9]. Ischemic strokes account for 87% of all total strokes, and 10% of these events are attributed to intracranial atherosclerosis[8]. Angioplasty and subsequent stenting of atherosclerotic neurovasculature are available to treat the risk of ischemic stroke in patients that are unresponsive to alternative therapies like anticoagulation medications and blood pressure/cholesterol therapies. Intracranial angioplasty and stenting are only performed on high-risk patients as a last resort because neurovascular stents have only received humanitarian device exemption from the Food

This thesis follows the style of Journal of Applied Polymer Science.

and Drug Administration (FDA)[9] due to limited success in clinical trials.

The current standard for treating endovascular diseases, including different types of atherosclerosis and coronary artery disease, are catheter-based stents. The current FDA approved stents are metallic and have evolved from bare metal stents to more advanced stents, some of which have drug eluting polymeric coatings[10]. Despite the success of current stent designs, they still have drawbacks. For example, these devices are no longer needed after the healing and remodeling of the vessel in which they are deployed. The permanent nature of traditional bare metal stents is a detriment, causing prolonged irritation and inflammation of the vessel that can lead to restenosis[11, 12]. Drug eluting stents were developed to help alleviate the problem of restenosis, but delayed healing due to polymeric coatings increases the chance of late thrombosis[13]. Another drawback of metal stents is that they can interfere and create artifacts when using imaging modalities such as magnetic resonance imaging (MRI) and computed tomography (CT)[14, 15]. Finally, the permanence of metal stents prevents further interventions on the same vessel and restricts natural vasomotion.

Metal stent drawbacks have motivated research in biodegradable polymeric stents[16, 17]. Polymer stents offer solutions to many of the problems associated with traditional metal stents. Biodegradation, for which the polymer chemistry can be tailored, after vessel remodeling and initial healing allows the vessel to completely endothelialize, restore its natural vasomotion, decreases the risk of late thrombosis, and allows for further

intervention on the diseased vessel or downstream vessels if necessary[12]. A predominant criticism of polymer stents is that they have inferior mechanical properties when compared to their metal counterparts due to polymers typically having a modulus that is three to six orders of magnitude lower than metals depending on if the polymer is in its glassy or rubbery state. However, studies have shown that polymer stents with modified geometries can achieve a structural response comparable to metal stents[17, 18], and other studies suggest that a lower modulus material may actually be more beneficial due to better compliance matching with the vessel wall[19]. These stents have potential in all areas where stents are currently used, but are particularly interesting for neurovascular applications due to their flexibility. Devices made of flexible low modulus materials will be able to navigate the tortuous vasculature of the brain easier. However, polymer stents are not without limitations. For instance, degradation products from biodegradable polymers such as poly-l-lactic acid can produce an acidic environment that causes prolonged inflammation[20]. Additionally, polymer stents must be designed with thicker strut geometries to achieve radial expansion forces comparable to metal stents. These thicker cross-sections limit the strains the devices can withstand[21]. Another inherent drawback of polymer devices is that polymers are not radio-opaque without modifications. The lack of radio-opacity can be alleviated with techniques such as adding radio opaque markers (e.g. gold[16]) or doping with tungsten[21]. These drawbacks require the optimization of polymer chemistries to have appropriate degradation times, biocompatibility, and mechanical properties. This study focuses on material mechanical properties and how they relate to device performance.

Shape memory polymers (SMPs) are relatively new materials that are attractive for medical devices, particularly stents[4-7, 22]. These materials can change their geometry when exposed to an external stimulus. This shape recovery can be induced in several ways (e.g. pH, electricity, heat), but this study focuses on thermal stimulation. Instead of elastic recoil, these devices return to their primary shape due to an entropy-driven process. This shape memory effect arises from netpoints (physical or chemical crosslinks) that remember the primary geometry and switching segments (amorphous or crystalline polymer regions) that can be "programmed" into a metastable secondary geometry. Amorphous switching segments actuate around a glass transition temperature (T_g), while crystalline switching segments actuate according to the melt transition temperature (T_m). The materials in this study are chemically crosslinked amorphous SMPs that actuate at T_g. Figure 1 portrays one thermal shape memory cycle. The cycle starts with the polymer in its primary shape. The polymer is fabricated in this geometry, and it is the lowest energy state because the polymer chains are highly coiled and randomly configured (max entropy state). When the material is heated above T_g, the amorphous polymer chains in the material loosen and are easily deformed. When the ribbon is deformed into the spiral geometry shown, the polymer chains within the material uncoil and become more aligned. This is a higher energy state because there is a decrease in entropy. Cooling the material below T_g while maintaining the load locks this secondary geometry. Below T_g, the polymer chains are not flexible enough to return to the max entropy state. Thus, potential energy is stored in the form of an "entropic

spring." In the last step of the cycle, the polymer chains coil when the material is heated above T_g, releasing the stored energy and returning the polymer to its primary geometry.

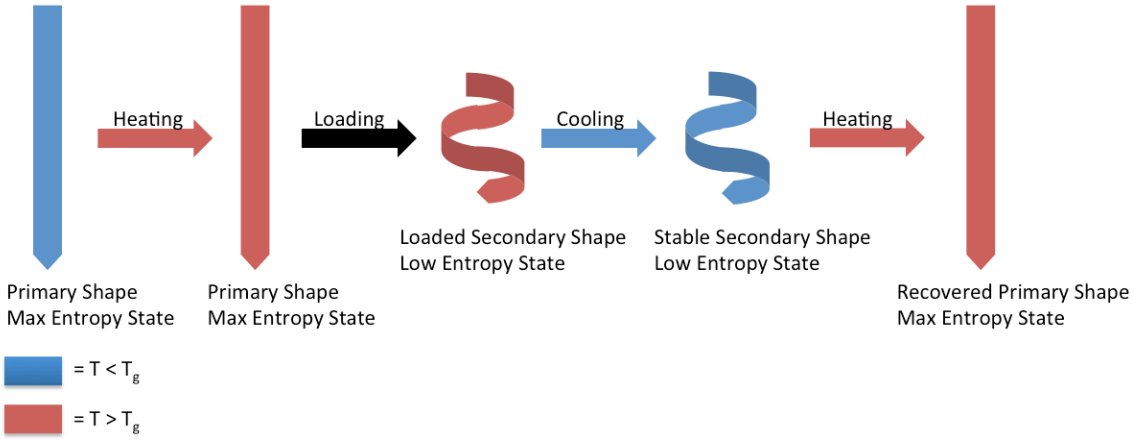

Figure 1 An idealization of one shape memory cycle of a shape memory polymer ribbon. This ribbon can be deformed when the temperature is above T_g, then cooled to below T_g to fix the secondary shape. Potential energy is stored at this step in the form of an "entropic spring." When the material is heated above T_g, this energy is released and the material returns to its primary shape.

Shape memory polymers can be heated by a variety of methods including laser light[5], magnetic induction[23], resistive heating, and body heat. These materials are useful for stent design because it allows them to be crimped to a small geometry and deployed via a controlled stimulus. This delivery method eliminates the need for balloon catheter device delivery, which can potentially overinflate and cause damage to the vessel[10].

Research objective

This study will expand on the clinical efficacy of a previously proposed SMP stent design[18] by characterizing its recovery behavior and quantifying the longitudinal flexibility of the device by performing three point bend tests, the results of which will be

compared to data from numerous stent systems that have been compiled and published[24]. This SMP stent design capitalizes on the flexibility of polymer devices in an effort to bridge the clinical gap for treating intracranial atherosclerosis. This flexible design is proposed to navigate tortuous neurovasculature, and has a collapse pressures comparable to current neurovascular stents[18].

A novel polyurethane shape memory polymer system developed by Keith Hearon will be used to achieve the complex geometry of the proposed stent design. This novel SMP system enables the fabrication of devices with the desired shape memory properties of thermosets using the superior processing capabilities of thermoplastics. One major advantage of thermoplastic polymers is in the area of processing. Thermoplastic polymers contain physical crosslinks such as hydrogen bonding and van der Waals forces. These physical interactions can be interrupted with elevated temperatures or a proper solvent, causing the polymer to flow. Thus thermoplastics can be easily processed into complex geometries using techniques such as heat extrusion and solution casting. On the other hand, covalently crosslinked thermoset polymers, whose mesh-like molecular structure resembles that of a fishing net, neither flow at elevated temperatures nor dissolve in solvents and are therefore subject to numerous processing limitations. However, covalent crosslinking can enhance certain mechanical properties, including higher failure stresses and better shape memory properties, and certain applications demand the enhanced mechanical advantages of thermoset materials. The novel SMP system used for stent fabrication in this study can be solution cast into a desired

geometry as a thermoplastic and subsequently crosslinked in a secondary step. In this SMP system, outlined in figure 2, thermoplastic polymers are solution blended with proprietary crosslinker monomers. These thermoplastic/crosslinker blends are subsequently subjected to ultraviolet (UV) radiation in the presence of photoinitiator to enable the formation of covalent crosslinks between the polymer chains. This process facilitates the construction of a complex thermoplastic geometry and the subsequent UV crosslinking to yield a final thermoset device.

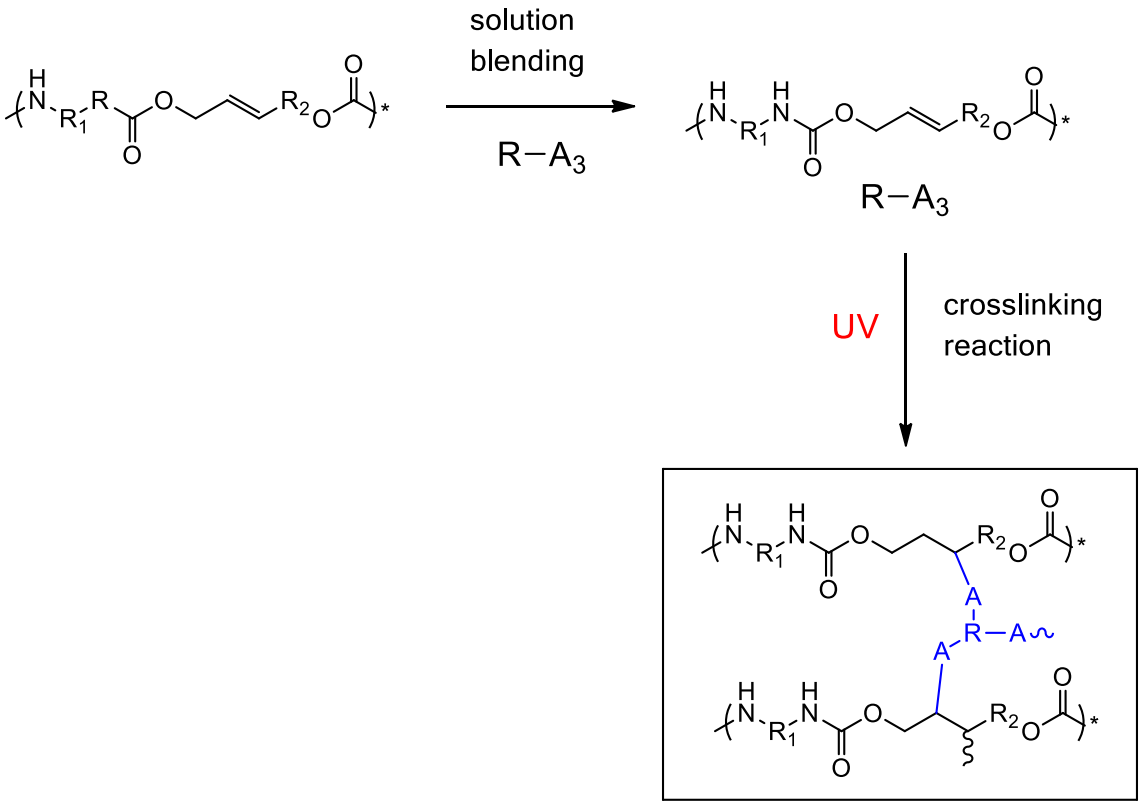

Figure 2 A thermoplastic polymer with a reactive double bond in the backbone is solution blended with a proprietary polyfunctional crosslinker. The polymer has significant processing flexibility at this point. Once the device geometry is made, the polymer is covalently crosslinked using ultraviolet radiation to initiate the crosslinking reaction.

This polymer system also allows for highly tailored mechanical properties, demonstrating independent control of T_g and rubbery modulus by altering the chemistry composition. Other benefits of this polymer system are sharp glass transitions and high rubbery moduli, which translate to fast shape recovery and higher recovery forces, respectively. This chemistry could be manipulated to be biodegradable, and post-processing techniques could be employed to make this material radio-opaque; however, both of these material aspects are outside the scope of this study.

CHAPTER II

METHODS

This study started with synthesizing thermoplastic urethanes. These polymers were used to identify a chemistry that was reproducible and compatible with a dip-coat processing technique. Polymer molecular weight, proprietary crosslinker percentage, and crosslinker chemistry were varied in thermoset film syntheses to find a functional material composition. Stents of varying wall thickness were made with a single chosen composition, and these devices were thermo-mechanically characterized with longitudinal flexibility and radial expansion tests.

Thermoplastic polymer synthesis

All chemicals, unless otherwise stated, were purchased from TCI America and used as received. Thermoplastic polyurethanes were synthesized from 2-butene-1,4-diol (2-but) and trimethylhexamethylene diisocyanate (TMHDI) in 33 wt% anhydrous tetrahydrofuran (THF) solutions in flame dried 8 oz glass jars using a 1 mole % stoichiometric diisocyanate excess. Figure 3 shows the polymerization reaction and resulting polymer repeat unit.

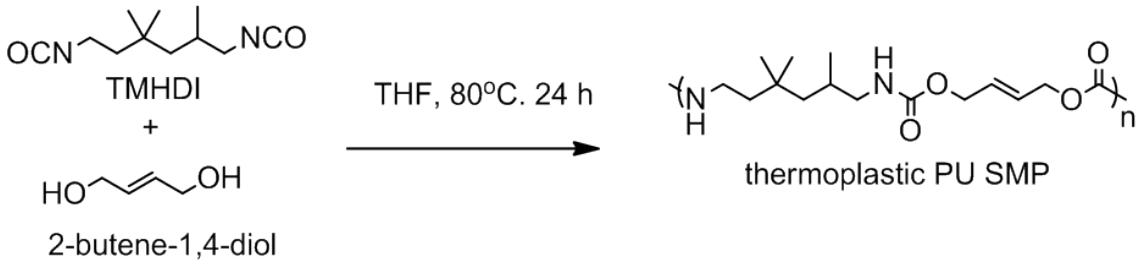

Figure 3 Trimethylhexamethylene diisocyanate and 2-butene-1,4-diol were polymerized in 33 wt% THF solution to yield polyurethane repeat units containing reactive double bonds.

All syntheses were conducted in 100 gram batches in the presence of 0.01 weight percent Zirconium(IV) 2,4-pentanedionate catalyst. The monomers were stored and mixed in a moisture-free environment using a LabConco glove box. All reactants, solvents, and catalysts were mixed in flame dried 240 mL glass jars, and 30 grams of 3 Å molecular sieves, purchased from Sigma Aldrich, were added to further reduce moisture content. To control the molecular weights of the polymers, allyl alcohol (AA) was substituted for the 2-but monomer in 1, 3, and 5 mole % quantities to serve as a monofunctional chain terminating agent. All polymerizations were carried out at 80°C for 24 hours at 120 RPM vortex speed using a Labconco RapidVap apparatus. After the polymerizations, the THF/polymer solutions were diluted to 10 wt % and were separated from the molecular sieves by filtration through VWR grade 490 filter paper. The filtered dilute solutions were then poured into 22 x 30 cm polypropylene dishes for solvent removal. The polypropylene dishes were left at ambient temperature and pressure in a fume hood for 12 hours, after which they were heated to 80°C for 24 hours, after which they were subjected to evacuation at 1 torr at 80°C for an additional 24 hours. After

solvent removal, clear thermoplastic polyurethane films were removed from the polypropylene dishes.

Size exclusion chromatography

Size exclusion chromatography (SEC) was conducted to quantify the molecular weights of the resulting polymerizations. SEC was conducted on a Waters 1515 HPLC equipped with a Waters 2414 differential refractometer, Waters 2998 photodiode array detector, and a three column series of PL gel 5 μm mixed C, 500 Å, and 104 Å (300 × 7.5 mm) columns. The system was equilibrated at 35°C in N,N-dimethylformamide, which served as the polymer solvent and eluent with a flow rate of 1.0 mL/min. Polymer solutions were prepared at a known concentration (ca. 3 mg/mL), and an injection volume of 200 μL was used. In addition, the differential refractometer was calibrated with standard polystyrene reference material (SRM 706 NIST), of which the specific refractive index increment dn/dc is known (0.184 mL/g). The differential refractometer response was used to determine the dn/dc values of the analyzed polymers. Single samples of thermoplastic PUs with 0%, 1%, 3%, and 5% allyl alcohol content were run.

Thermoset film fabrication

Thermoset films were fabricated by solution blending 3.33 g of the thermoplastics containing varying allyl alcohol content with varying amounts of the proprietary crosslinkers, Crosslinker A and Crosslinker B, in 15 wt% THF solutions. These samples were made to identify a chemistry that was stable in solution at high concentrations

because initial stent fabrication efforts yielded phase separated material. Table 1 outlines the composition of each series. The crosslinker percentages refer to the ratio of moles crosslinker reactive sites to moles of C=C groups in the thermoplastics (provided the information that one proprietary crosslinker reactive group reacts with one C=C group). Three wt % of the photo initiator 2,2-Dimethoxy-2-phenyl-acetophenone (DMPA) was used for every solution to ensure sufficient crosslinking.

TABLE I
Summary of Thermoset Film Compositions Varying Crosslinker Chemistry and Concentration With Varying Allyl Alcohol Content Thermoplastic Polymer

Series Number	Sample	Allyl Alcohol Content	Crosslinker A Content	Crosslinker B Content
1	A	0%	100%	0%
	B	1%	100%	0%
	C	3%	100%	0%
	D	5%	100%	0%
2	A	0%	0%	100%
	B	1%	0%	100%
	C	3%	0%	100%
	D	5%	0%	100%
3	A	5%	25%	0%
	B	5%	50%	0%
	C	5%	75%	0%
	D	5%	100%	0%
4	A	5%	0%	20%
	B	5%	0%	40%
	C	5%	0%	60%
	D	5%	0%	80%
	E	5%	0%	100%

Solutions containing thermoplastic polymer, crosslinker, and photoinitiator were poured into 5 x 5 cm reservoirs in 12-compartment polypropylene boxes purchased from McMaster-Carr. Films were cast by allowing solvent to evaporate for 24 h at ambient temperature in a fume hood. The films were subsequently crosslinked for 45 minutes in a UV crosslinker (UltraViolet Products) at a wavelength of 365 nm. The films were transferred into aluminum trays and post-cured at 120 °C under vacuum for 2 hours. The optical clarity of each film was observed for signs of phase separation. The clearest sample chemistries were chosen for further quantification of homogeneity and thermo-mechanical behavior.

Dynamic mechanical analysis (DMA)

The thermoset films were cut into thin rectangular DMA samples (approximately 4.75mm x 32mm) using a Gravograph LS100 CO_2 laser engraving system. Dynamic mechanical analysis of these samples was performed in tension using a TA Q800. Tests were conducted using the multi-frequency strain mode with a preload force of 0.01 N. Samples were equilibrated at 0°C, held isothermal for 10 min, and temperature was ramped from 0°C to 120°C at 1°C/min. The measured dynamic material properties (i.e. storage modulus, loss modulus, and tan delta) were plotted as a function of temperature. These plots were analyzed to determine glassy modulus, rubbery modulus, and T_g as defined by the tan delta peak.

Tensile testing

Strain to failure tests were conducted on an Instron 5965 test frame with an accessory Eurotherm temperature chamber and video extensometer for measuring strain. Solution cast thermoset films were cut into ASTM D638 Type V dogbones using the LS100 CO_2 laser. Each sample was sanded with 400 grain sand paper to remove surface defects. The samples were strained to material failure at a rate of 50 mm/min at the tan delta peak temperature as determined by DMA.

Shape memory tests

Two types of tensile shape memory tests were attempted to acquire material properties that would be necessary to calibrate a computational SMP model. The tensile tests were modeled after those conducted by Volk et al[25]. Unfortunately these methods did not work for thin dip-coated tensile samples. These tests will need to be expanded in the future to get consistent results. A third shape memory test was conducted to prove the shape memory properties of the stent prototypes.

Tensile constrained recovery tests

In this test, material is heated above T_g, stretched to a fixed strain, cooled below T_g, and unloaded to fix the elongated secondary geometry. The sample is then re-gripped at a fixed strain and heated above T_g to measure the stress the material exerts during shape recovery as a function of temperature. To accomplish this, Type V dogbone samples were gripped in the top grip of an Instron 5965 test frame and equilibrated at 80°C for 15

minutes. This temperature was chosen because it is well within the rubbery plateau of the material. After reaching thermal equilibrium and zeroing the load cell, the bottom of the sample was gripped. Samples were strained to 25% as measured by a video extensometer and subsequently cooled, maintaining the 25% strain, to 20°C at a rate of 1°C/min. The samples were unloaded to zero stress. This relieved any internal stresses due to thermal expansion during the test, but the material still remained in its elongated secondary shape because it was below T_g when it was unloaded. The sample was re-gripped, and recovery stress was measured while the samples were held at constant strain and the temperature was ramped back to 80°C at 1°C/min. A plot of stress as a function of temperature was generated to determine the recovery stress of the material.

Tensile free recovery tests

This test is similar to the constrained recovery tests, but after the material is programmed into its secondary geometry, the sample is allowed to hang freely as it is heated above T_g. This test quantifies the amount of strain a shape memory material can recover. The free recovery tests followed the same method as the constrained recovery tests up thru when the samples were unloaded to zero stress. At this point, the bottom grip was released to ensure zero applied load on the sample. Strain recovery was measured by the video extensometer while the temperature was ramped back to 80°C at 1°C/min. Plots of strain recovery as a function of temperature were generated to determine the amount of the applied strain that was recovered.

Stent fabrication

Stents of a complex geometry were made using a dip-coating procedure. First, cylindrical pins were dip-coated in a polymer solution and then machined into a complex geometry using a CO_2 laser.

Dip-coat solution

The dip-coat solutions were prepared in 60 mL glass vials by dissolving 22 g of the 5% AA thermoplastic polyurethane in 27 g THF. This concentration of polymer and solvent was qualitatively optimized in multiple dip-coating trials to achieve desirable viscosity and volume for dip coating. To match the dip-coat solution to the chosen chemistry from the thermoset film trials, Crosslinker A was added to the solution to make a 2:1 mole ratio of polymer double bonds to crosslinker reactive site functionalities. Since the reduced molecular weight thermoplastic PUs are telechelic, the double bonds from the allyl alcohol chain ends were accounted for in the stoichiometry. Three weight percent DMPA was added to the polymer solutions after thermoplastic dissolution. After photoinitiator addition, all solutions were wrapped in aluminum foil to minimize exposure to ambient light.

Dip-coating

Brass pins measuring 4 mm in diameter were cut into 80mm lengths. These pins were mounted in a drill press and sanded to a smooth, tarnish-free finish using 400 and 2000 grit sandpaper. To ensure the material would release from the pin, a thin coat of Teflon

mold release spray was added to each pin. The spray was then sintered to the pin using a handheld butane torch. As shown in Figure 4, a group of four pins were mounted on a custom fixture for dip-coating and then dipped, using a linear translating platform, into the polymer solution over a 51 mm range at a rate of 0.67 mm/sec. The pins were held at the bottom of the dip for 20 seconds, and removed from the solution at the same rate. Before applying another dip-coating layer, the pin fixtures were placed in an oven at 45 ˚C for 20 minutes to promote solvent evaporation. The dipping process was repeated 6 to 10 times to vary the wall thickness of the polymer tubes between 140-220 microns.

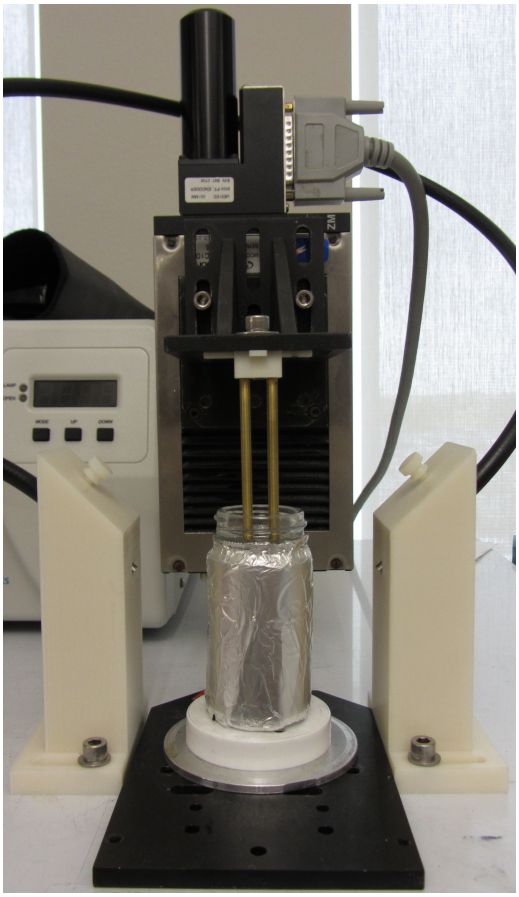

Figure 4 Dip-coating setup shown at the top of the dip. The ends of the pins are just above the surface of the polymer solution.

In addition to pins, flat brass bars measuring 3 x 80 x 12 mm were dip-coated to yield flat films with the same thickness and processing history as the stent material. These were used to make DMA and tensile samples because they are more representative of the stent material. The solution cast thermoset films proved to have different mechanical properties, which will be covered in the discussion.

Processing

After dip-coating, the pins were left in darkness for 24 hours to allow further solvent evaporation. Allowing for some solvent evaporation reduces the amount of material shrink during the post cure, which minimizes material splitting. However, leaving the pins at ambient conditions for too long (multiple days) can lead to phase separation of the blended crosslinker. The pins were crosslinked for 45 minutes in a UV crosslinking chamber at a wavelength of 365 nm. Figure 5 outlines the crosslinking mechanism of the stent material composition.

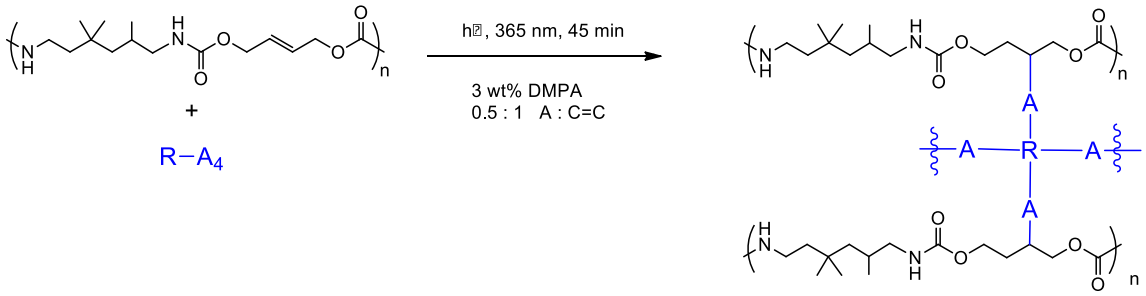

Figure 5 Crosslinking chemistry outline. The dip-coated thermoplastic polymer material is solution blended with polyfunctional Crosslinker A in a 0.5:1 A : C=C ratio. The photoinitiator DMPA is also solution blended at 3 wt% to initiate polymer crosslinking.

As shown in figure 6, the final crosslinked material was then cut into solid rings as well as complex stent geometries using a LS100 CO_2 laser equipped with a cylindrical engraving attachment. The stent pattern was made using SolidWorks 2011 and saved as an .ai file type. Using Adobe Illustrator, this file was converted to an .eps file, which is compatible with the LS 100 Gravostyle software. After engraving, the material was post cured on the brass pins at 120˚C for 2 hours under vacuum to remove residual solvent. Finally, the stents were carefully removed by hand from their brass dip coating pins. All thermoplastic polymers, thermoset films, stents, and tubes were kept in sealed containers that contained desiccant rocks to prevent moisture uptake. Water plasticizes thermoset samples, compromising their shape memory behavior, and unwanted contribution of moisture mass when weighing out thermoplastic samples can negatively affect the stoichiometry of reactions.

Figure 6 Dip coated pin after processing. The polymer is currently a semi-soft gel due to residual solvent. Post curing removes this residual solvent and yields the final material. The clarity of the material at the tip of the pin is indicative of favorable miscibility.

Sol/gel analysis

Sol/gel analysis experiments were conducted to quantify the amount of potentially leachable components left within the final stent material. These leachables are important to consider for material biocompatibility. Five vials were filled with approximately 50 mg of stent pieces and dried under vacuum at 80°C for 24 hours. After drying, the polymer mass was recorded and THF was added to the vial to yield a 1:150 polymer to THF ratio. The vials were oscillated at 50°C for 24 hours. The swollen stent samples were removed from solution, transferred to new vials, and dried under vacuum at 80°C for 24 hours. The final polymer masses were recorded and the gel fraction was quantified according to the following equation:

$$(1) \qquad Gel\ Fraction = \frac{w_f}{w_o}$$

Where w_f is the final sample weight, and w_o is the initial sample weight.

Three point bend tests

To quantify their ability to navigate tortuous vessels, stent prototypes with varying wall thicknesses were tested for their longitudinal flexibility using a TA Q800 Dynamic Mechanical Analyzer in the 3 point bending mode. The stents were tested at room temperature (23 °C) for comparison to other published data[24], and at 37°C to analyze the performance of the device at body temperature. The expanded devices were held at the testing temperature for five minutes to reach thermal equilibrium. The 4 mm diameter devices were bent to a displacement of 1.2 mm at a rate of 5 mm/min, and then returned back to zero displacement at the same rate. This method was adapted from the ASTM F206-08 standard for testing stents and stent systems[26] with modifications to accommodate the geometry of the DMA three point bending fixture. The ASTM standard calls for a 2 mm displacement, but displacements beyond 1.2 mm caused the sample to hit a lower portion of the three point bending base, effectively reducing the span length from 20 mm to 13 mm. The span length was set to 20 mm to more accurately reproduce the method used by Ormiston et al.[24]. Longitudinal flexibility was determined by plotting static force versus displacement and interpolating the slope of the initial loading curve.

Radial force and recovery tests

These tests were conducted using a Blockwise RJA62 J-Crimp™ Radial Compression Station coupled to an Instron 5965 tests frame. The components of this system are outlined in figure 7. This system transduces the linear motion, the force of which can be measured by the load cell, of the tensile tester into radial expansion and compression on the specimen.

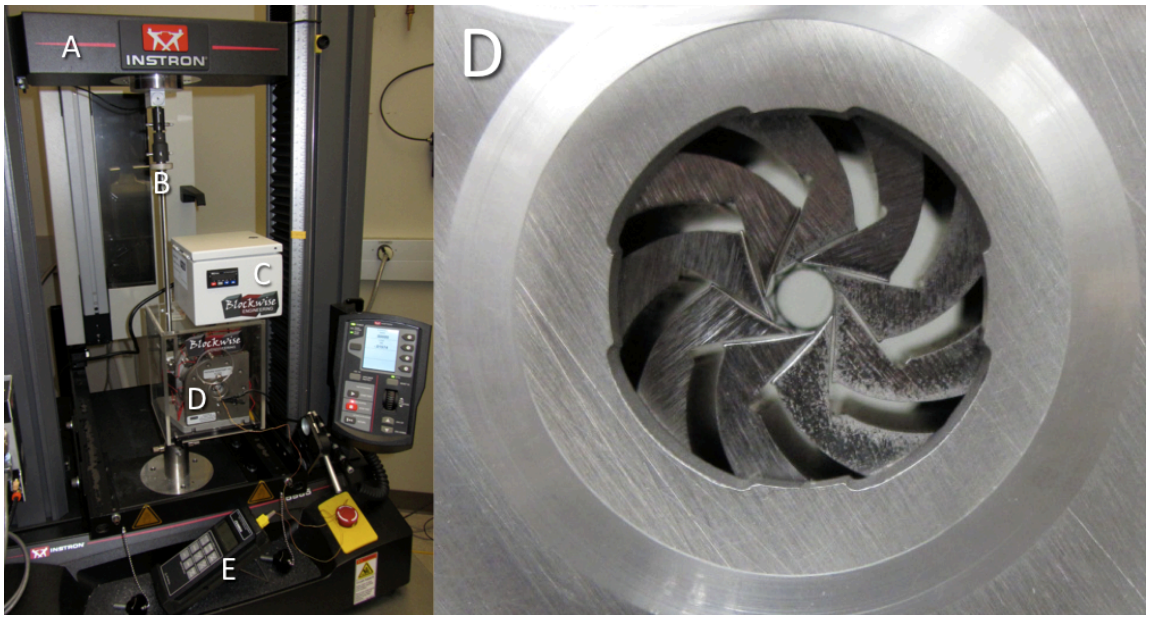

Figure 7 The left panel shows the full experimental setup for the radial force experiments. The tensile testing frame (A) is connected via the tensile adapter rod (B) to the compression station (D). Temperature is controlled with the controller (C) and monitored in real time with a thermocouple (E) placed concentrically in the compression station. The right panel is a close-up of the nine compression dies.

The mechanical relationship between the radial and linear behavior of this system can be defined by the following equations, which were provided by the device manufacturer:

(2) $$\Delta D = 0.7374 \cdot \Delta X$$

(3) $$TRF = 2.712 \cdot F$$

(4) $$P = \frac{145.04 \cdot TRF}{\pi \cdot D \cdot L}$$

Where ΔD is the change is sample diameter; ΔX is the movement of the tensile tester crosshead; TRF is the total radial force that the sample exerts on the nine dies of the crimping station; F is the force measured by the testing frame; P is the pressure exerted on the sample in pounds per square inch (PSI); D is the diameter of the sample; and L is the length of the sample.

Crimping force and controlled expansion tests

Stent prototypes were placed in the compression station and equilibrated to the testing temperature of 55˚C or 70˚C for one hour. Each sample was crimped from the initial, open diameter of ~4 mm to a final diameter of 1.4 mm over a period of one minute. The crimp was held for thirty seconds to let the material equilibrate if it is substantially visco-elastic. The crimping station was opened back to the original diameter over a period of one minute to match the loading profile. The crimping and radial expansion behaviors of these devices were quantified by plotting pressure as a function of crimping percentage, which is defined by the following equation:

(5) $$Crimp\% = \frac{\phi_o - \phi}{\phi_0 - 1.4}\ x\ 100$$

Where ϕ_o is the original stent diameter, and ϕ is the current stent diameter. This measurement is a quantification of the crimp amount, with a 1.4 mm final diameter being 100% crimped. This is not a quantification of the percent reduction in overall device diameter. Stents with wall thicknesses of 140, 180, and 220 microns were tested at T_g (55˚C) and 70˚C. It is useful to know the crimping behavior at 55˚C because it is

the tan delta peak, which is the temperature for theoretical max strain. Recovery behavior at 70˚C will be useful to know because this temperature is within the rubbery plateau of the material, indicating full shape recovery.

Constrained radial recovery

Polymer tubes with 4.26 ± 0.02 mm diameters, 5.85 ± 0.01 mm lengths, and 150 micron thicknesses were crimped using a Machine Solutions Inc. SC 150 stent crimping station. The tubes were loaded in the crimping head and equilibrated at T_g for one hour. The stents were crimped to a final diameter of 1.4 mm using a gauge pin. To fix the temporary shape, the crimping head was held fixed and cooled to room temperature over a period of two hours. The tubes were removed from the crimping station and placed into the Blockwise compression station tensile adapter at room temperature. The compression station diameter was set to a specific crimping percentage according to the following equation:

$$\phi_{test} = \phi_o - (\phi_0 - 1.4) \cdot \frac{Crimp\%}{100} \quad (6)$$

Where ϕ_{test} is the station diameter during the test. Temperature was ramped from room temperature to 70˚C in order to measure the recovery force of the tubes through the full glass transition and into the rubbery plateau of the material. Temperature was sampled every 10 seconds using a stopwatch and a thermocouple placed concentrically within the compression station. The thermocouple was necessary because this system is designed for equilibrated temperature testing, and there is a significant difference (10-15 degrees) between the controller readout and the actual temperature of the compression dies during

portions of the heating profile. Constrained recovery was quantified by plotting pressure vs. temperature of tubes recovering to 100, 80, 60, 40, and 20 crimping percent. All tests were run at least twice to verify the repeatability.

Stent shape recovery

Stent prototypes were crimped over a wire using the same method described above in the constrained recovery tests. The crimped stent was placed in a water bath at 70˚C and the shape recovery was filmed using a digital camera.

CHAPTER III

RESULTS

Thermoplastic polymer syntheses

Table 2 outlines the Size Exclusion Cromatography results of the synthesized thermoplastic polymers. Results are given as number average molecular weight (M_n), weight average molecular weight (M_w), and polydispersity index (PDI), which is the ratio of the two (M_w/M_n).

TABLE 2
Thermoplastic Polymer SEC Results

% Allyl Alcohol	M_n (g/mol)	M_w (g/mol)	PDI
0	97600	221400	2.27
1	63500	131000	2.06
3	36600	61900	1.69
5	29500	50800	1.72

Increasing allyl alcohol content shows clear a trend in lowering polymer molecular weight. Smaller polymer chains are more soluble in solvent, and should be more miscible in solution with the proprietary crosslinkers. Additionally, increasing allyl alcohol content results in a narrower polydispersity index (PDI). This means the polymer chains are becoming more consistent in length, which could result in a more homogenous polymer network after crosslinking. A more homogeneous network results in a narrower glass transition and thus, faster device recovery.

Thermoset films

Crosslinker A (f =4) and Crosslinker B (f=3) were selected in accordance with the work done by Keith Hearon. Phase separation of crosslinkers from the thermoplastic blends occurred during solution casting and increased with increasing thermoplastic molecular weight and increasing crosslinker composition. Samples without phase separation were achievable for samples with M_w < 100 kDa and with crosslinker compositions ≤ 50%. During phase separation, precipitation of the solution blended crosslinkers occurs, resulting in a lower stoichiometric ratio of crosslinker reactive sites : C=C groups than desired. Consequently, the phase separated samples have lower crosslink densities and altered mechanical properties. The two approaches for reducing phase separation were lowering the thermoplastic polymer molecular weight (described in the previous section) and reducing the molar content of the crosslinker. The polymers outlined in Table 1 were visually inspected for optical clarity. For the purpose of this study, samples with complete optical clarity as observed by close inspection by the naked eye were determined to have no phase separation. The clear samples with the highest molecular weight and crosslinker content were series 3B, the 5% allyl alcohol, 50% Crosslinker A composition. This composition was chosen for more quantitative mechanical analysis. Although Crosslinker B compositions yielded clear films when blended in up to 80% composition with 5% AA thermoplastics, this crosslinker was not selected because it was highly light sensitive. Since dip-coating can take several hours, a light sensitive crosslinker is not ideal for the proposed stent processing technique.

Dynamic mechanical analysis (DMA)

DMA experiments were performed on dip-coated and thicker solution cast films of the selected composition. Dip-coated films were ~120-200 microns thick, while the solution cast films were ~900-1200 microns thick. Figure 8 presents differences in the storage moduli and tan delta of the materials prepared by dip-coating or solution casting. The solution cast films exhibited a broader tan delta peak and a higher rubbery modulus than those of the dip coated films.

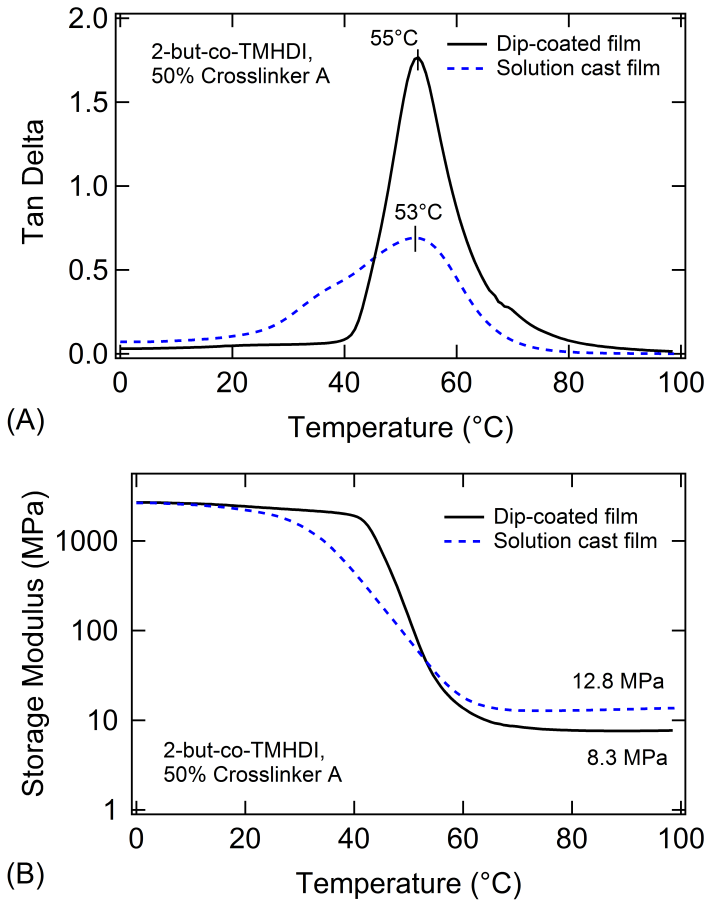

Figure 8 DMA results for dip-coated and solution cast films. (A) The broader tan delta peak of the solution cast sample indicates that this sample had less network homogeneity than the dip-coated sample. (B) The solution cast films exhibited a 50% higher rubber modulus value when compared to the dip-coated films.

The breadth of the glass transition region of a polymer is indicative of network homogeneity. Glass transition breadth can be measured by the sharpness of the tan delta peak, which is determined by DMA testing and is often quantified in the literature by calculating the full width half maximum (FWHM) value of a tan delta peak[27]. With a FWHM value of 12.6 ˚C, the dip-coated films demonstrate substantially higher network homogeneity when compared to solution cast films with a FWHM of 26.9 ˚C. For many SMP applications, sharp glass transitions are desirable because the SMP remains glassy until it is heated to a temperature very close to its T_g, thus enabling high degrees of shape fixity until heating to a desired, specific actuation temperature. By this qualification, the DMA results indicate that the dip-coated samples are more desirable for a stent application than the solution cast films. The 50% higher rubbery modulus of the solution cast films allows for greater device recovery force, but this comes with the trade off of less strain to failure. Since crimping strains are already limited by thicker strut cross sections, a lower rubbery modulus could be advantageous in the case of this stent application. Based on the thermal history and preparation techniques of these samples, it is assumed that the dip-coated films are more representative of the stent material. Although these two samples are different thicknesses (Dip coated films ~ 150 microns, Solution cast ~ 1000 micron), these DMA tests are geometry independent and take the size of the sample cross section into account.

The reasons for the observed differences in dynamic moduli for the dip-coated versus solution cast samples are not fully understood at the present time, but they are being

investigated as part of a future publication for these materials. Preliminary results indicate that residual solvent content during crosslinking likely affects the crosslinking reaction kinetics; however, these considerations are beyond the scope of this study.

The tan delta peak temperature of 55˚C will be used as the T_g of the materials for this study. Since this T_g is above body temperature, these devices would require an external heating source for actuation.

Strain to failure

Strain to failure tests were conducted on dog bone samples at the tan delta peak temperature of 55ºC to determine the maximum strain capability of these materials. The data in figure 9 gives insight into the maximum deformation a device can undergo during crimping before the device fails. The average ultimate strain of the material is 1.16 ± 0.09, and average ultimate stress is 10.34 ± 0.85 MPa.

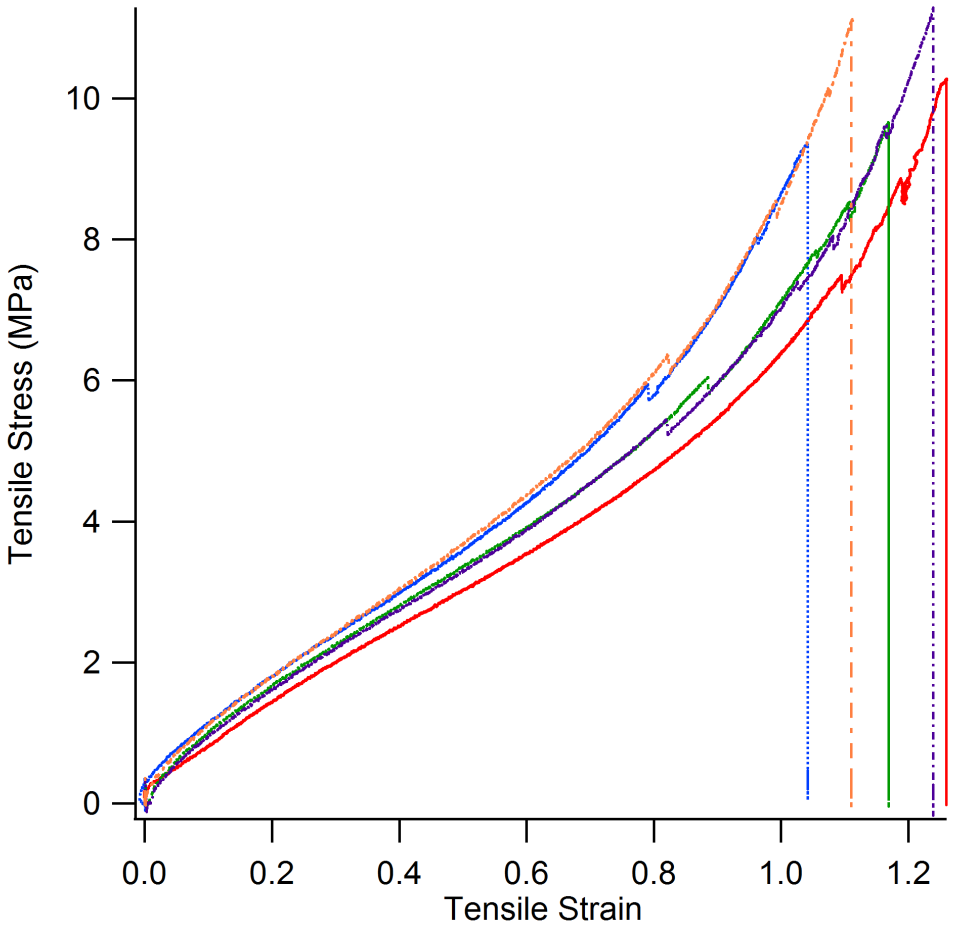

Figure 9 Strain to failure results at 55˚C. The different curves are duplicates of the same test to show repeatability. Average ultimate strain is 1.16 ± 0.09 and average ultimate stress is 10.34 ± 0.85 MPa.

To get a first order approximation of the crimping strains experienced by the device, the equation for beam bending strain can be applied:

$$\varepsilon = \frac{y}{r} \tag{7}$$

Where ε is the bending strain, y is the distance from the neutral axis, and r is the radius of curvature. The maximum tensile strain a crimped stent would undergo would be along the edges of a complete fold. A completely folded 220 micron tube would have a 220 micron radius of curvature, with the exterior edge (y = 110 microns) undergoing the

maximum strain. This situation yields a bending strain of 0.50, which is well within the material strain limit of 1.16. Crimping trials have proven that stents made of this material consistently crimp at 55°C without cracks or creases.

Stent prototypes

The final stent prototypes measured 25.51 ± 0.32 mm long and 4.29 ± 0.05mm in exterior diameter with wall thicknesses ranging from 140 to 220 microns depending on the number of dips (6-10 dips). However, control over thickness is relative to each round of dip-coating. Although this preparation technique consistently results in functional devices, it needs further optimization for more consistent thickness control. The primary problem for thickness control is solvent evaporation from the dip-coating solution, which changes the concentration and viscosity during the lengthy process. The laser-machined edges of the prototypes appear rough when observed under SEM (see bottom of the figure found on p. 34). These rough edges provide nucleation points for device failure at high strain, and provide more surface area for protein adhesion and biofouling. However, higher quality laser machining systems, such as an excimer laser, could be used to improve the edge quality of the stents. Figure 10 shows the device design and demonstrates the crimpability of the device. The design uses five rings connected by "s" shaped struts. The rings hold the vessel open, while the strut design allows for overall stent flexibility[18]. Figure 11 shows the device in closer detail.

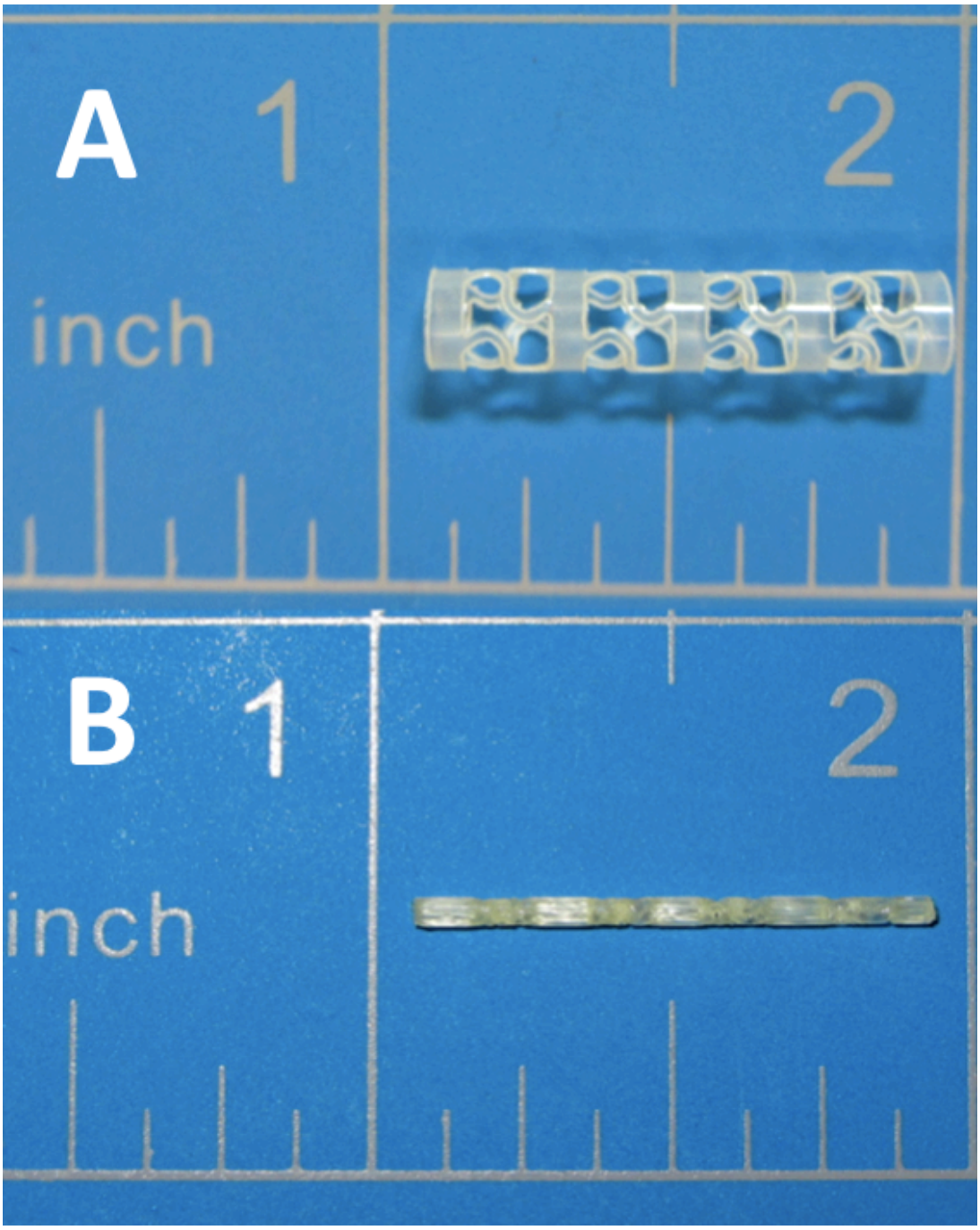

Figure 10 Images of a stent prototype with a 210 micron wall thickness in its (A) expanded state and (B) crimped state. Polymer opacity is due to residual Teflon from the dip-coating pin.

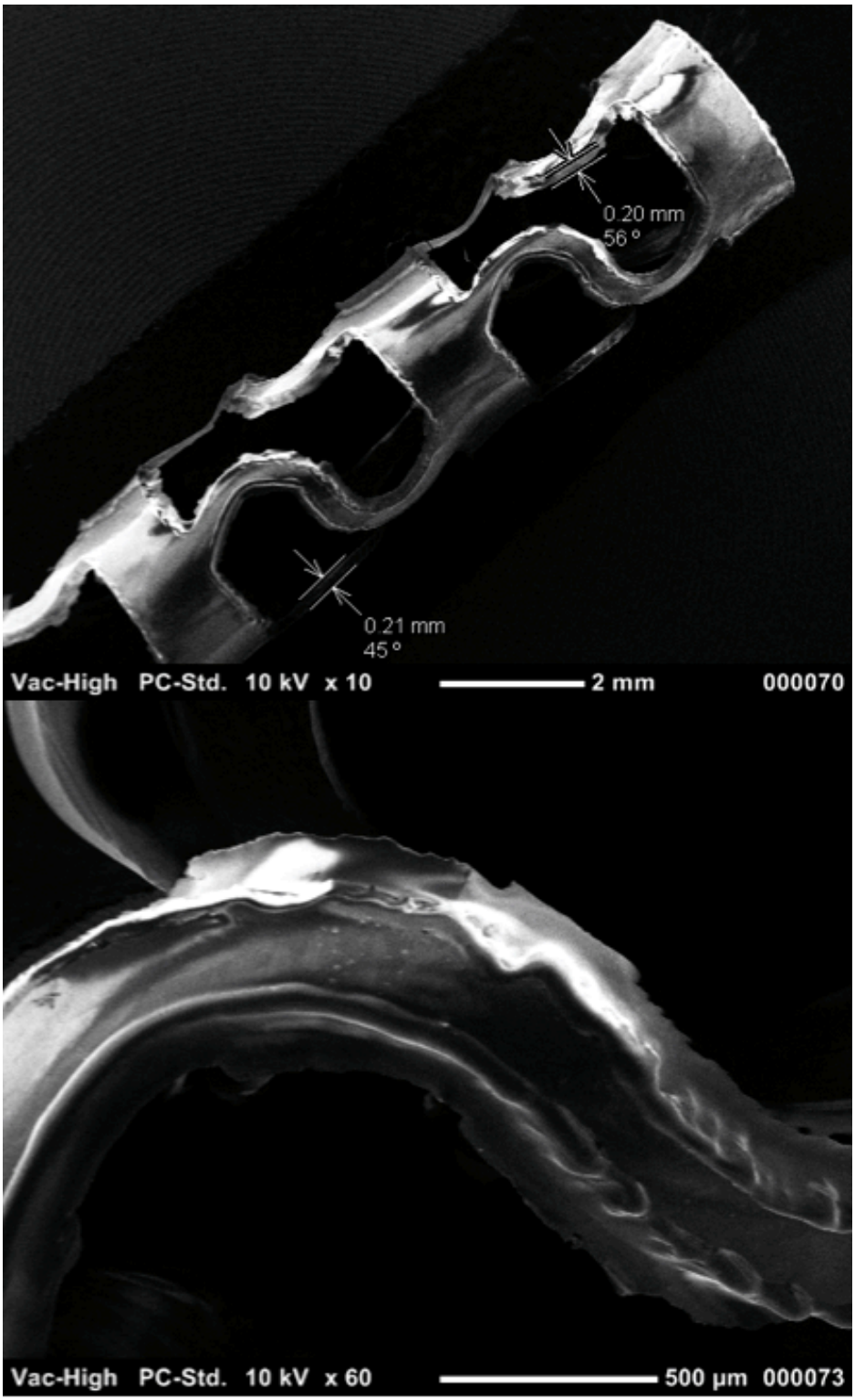

Figure 11 Scanning electron images of a stent prototype. The bottom panel is a close-up of a strut and shows the quality of the CO_2 laser cut.

Sol/gel analysis

The purpose of this gel fraction test was to quantify the amount of potentially leachable material still left within the crosslinked polymer. The gel fraction data is outlined in Table 3. The mass loss is likely due to uncrosslinked thermoplastic polymer chains, residual crosslinker, and photoinitiator that can escape the polymer network.

TABLE 3
Polymer Stent Gel Fraction Results (Average 0.92 ± 0.02)

Wo (mg)	Wf (mg)	Gel Fraction
47.8	43.9	0.92
48.8	44.5	0.91
52.8	48.4	0.92
53.5	51.6	0.96
44.6	42.1	0.94

With an average gel fraction of 0.92, this material could leach a considerable amount of material during the device lifetime. The identity and biocompatibility of this uncrosslinked material is not currently known, but it could possibly be detrimental to the body. However, changes to the fabrication and synthesis procedures can be made to get this gel fraction closer to the ideal value of 1.00. The gel fraction could be raised by using less photoinitiator (such as 1%), but only if the material properties are not significantly affected. Longer crosslinking and post cure times could also raise the gel fraction by ensuring more complete material reaction. Another approach would be to remove the leachables prior to device implantation via solvent swelling.

Three point bending

Figure 12 shows a clear trend that longitudinal stiffness increases with increasing wall thickness. Additionally, these devices have longitudinal stiffness values below or within the lower range of the stents reported by Ormiston et al[24]. This reference publication conducted 3 point bend analysis on devices with a diameter of 3.5mm, which is 0.5mm less than the devices in this study. This is an important note because diameter has a definite affect on longitudinal flexibility. In spite of this difference in diameter, the stiffness data in figure 12 shows that these devices could have potential in applications involving highly tortuous vasculature, such as in the brain. Figure 12 also shows that there is only a small difference between the room temperature and body temperature stiffness values, which is to be expected since the material is still in its glassy state at body temperature. The horizontal error bars are the average and standard deviations of stent wall thickness based on 5 measurements at each end of the stent. These bars are large because the material gets thicker along the length of the dip-coating pin due to the nature of the dip. A longer dip would provide a longer region of homogenous thickness, but the 51mm length of the dip-coating stage inhibits this. The thickness is more uniform when the sample is machined out of the middle of the dip, but this minimized the useable material for the study and was not always followed due to the need for more samples. There is no data point for the 220 micron devices at body temperature because all of the devices of this dimension were damaged in other tests, and the deadline of this study inhibited the fabrication of more devices to complete the figure.

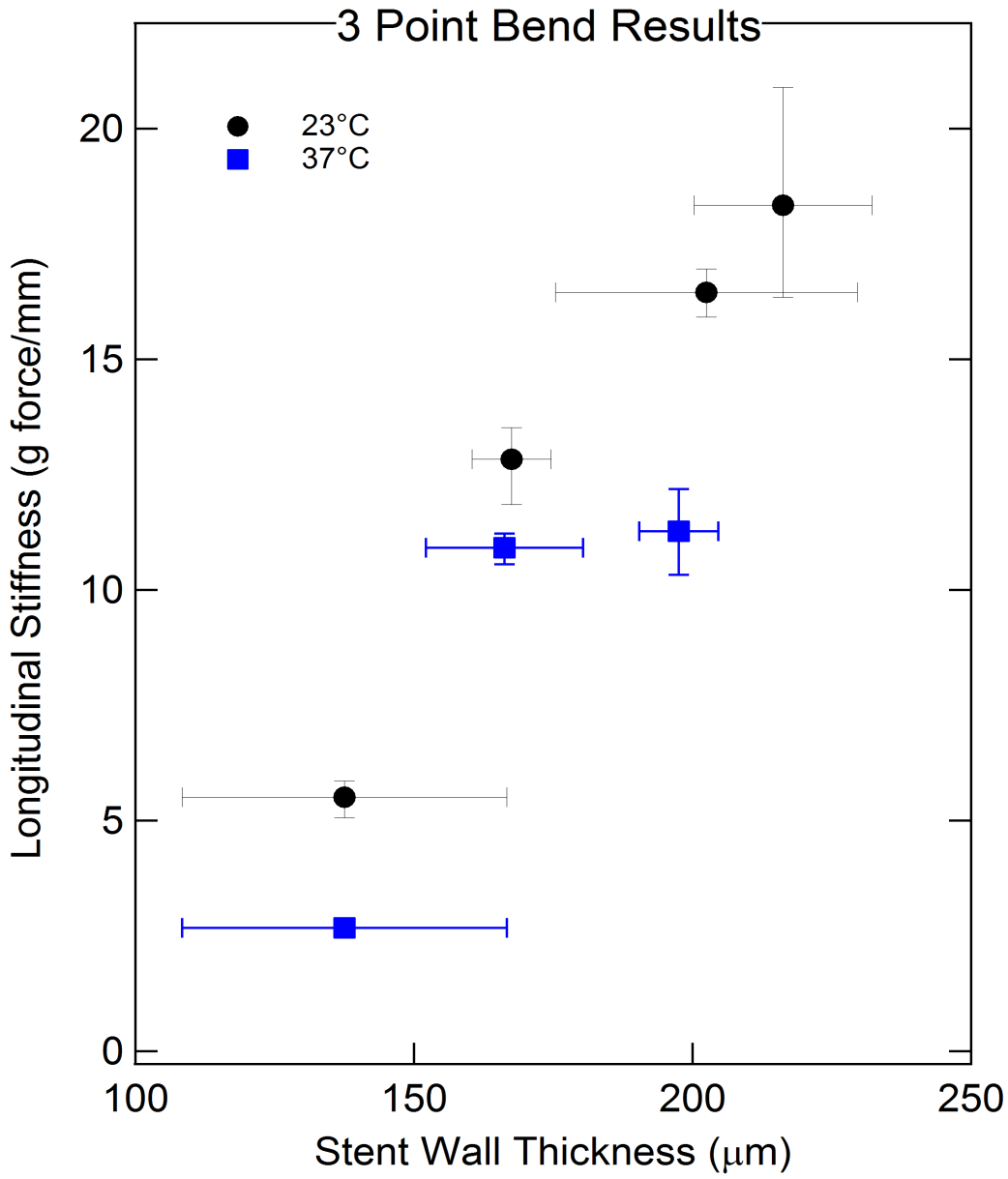

Figure 12 Three point bending results show increased longitudinal stiffness with increasing stent wall thickness. These devices exhibit longitudinal stiffness values below or within the lower range of currently available stent systems[24]. Vertical error bars are ranges (n=3) while horizontal bars are standard deviations computed from 5 measurements at either end of the stent.

Tensile shape memory tests

These tests were not successful. Ideally the samples for these tests would be ~1mm in thickness. It is possible to get this thickness by solution casting films, but as discussed in previous sections, the kinetics of the current solution casting method yields samples with mechanical properties that differ from the dip-coated material. Although dip-coated films had the desired mechanical properties, they were too thin for these tests to get consistent results.

Free recovery tests

These tests ran smoothly until the free recovery step. During material recovery, the video extensometer would lose correlation with the sample due to curling. This curling is likely due to minor temperature variations within the thermal chamber during heating. The samples are especially sensitive to minor temperature fluctuations because of their thin geometry. This curling effect could be minimized by thicker samples because a bigger cross section will resist out of plane bending, resulting in a more linear shape recovery that can be detected by the video extensometer.

Constrained recovery tests

A few constrained recovery tests were successful, but the material was only strained to 10%. Although this material can definitely withstand higher strains (according to figure 9), these tests were not pursued further due to time limitations. These tests were intended for future constitutive model calibration, but constrained recovery data is not useful

without complementary free recovery data. These tests will be possible once a consistent method for casting thicker films is created.

Stent recovery

As seen in figure 13, these devices display excellent shape recovery. A crimped stent fully recovers within one second when submerged in a 70˚C water bath. This quick deployment time will make it easy for physicians to hold the device in the correct place during device actuation. A fast delivery time also reduces the total amount of heat introduced into the neurovascular environment, which minimizes the potential for thermal tissue damage. A one second deployment time is an order of magnitude faster than other proposed stent systems deployed at body temperature with recovery times ranging from 10 seconds[4, 7] to 150 seconds[22]. Although this polymer system used in this study can be tailored to have a T_g around body temperature, ambient body heat actuation can cause device failure if the device deploys prematurely in the catheter, causing it to stick. Although a higher temperature deployment complicates the final device with a heating apparatus, it gives the clinician an additional level of control and increases the device working time.

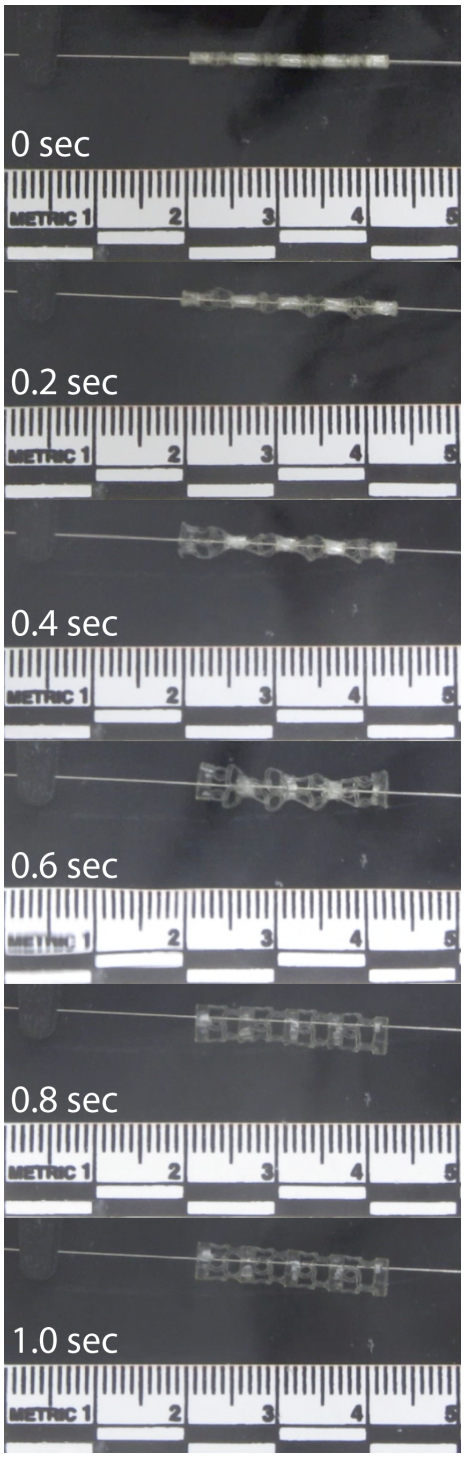

Figure 13 Time-lapse figure showing a recovering stent in a 70˚C water bath. Full recovery took place within one second.

Crimping force and controlled expansion

Figure 14 outlines the typical crimping and unloading behavior of the stent prototypes at a fixed temperature.

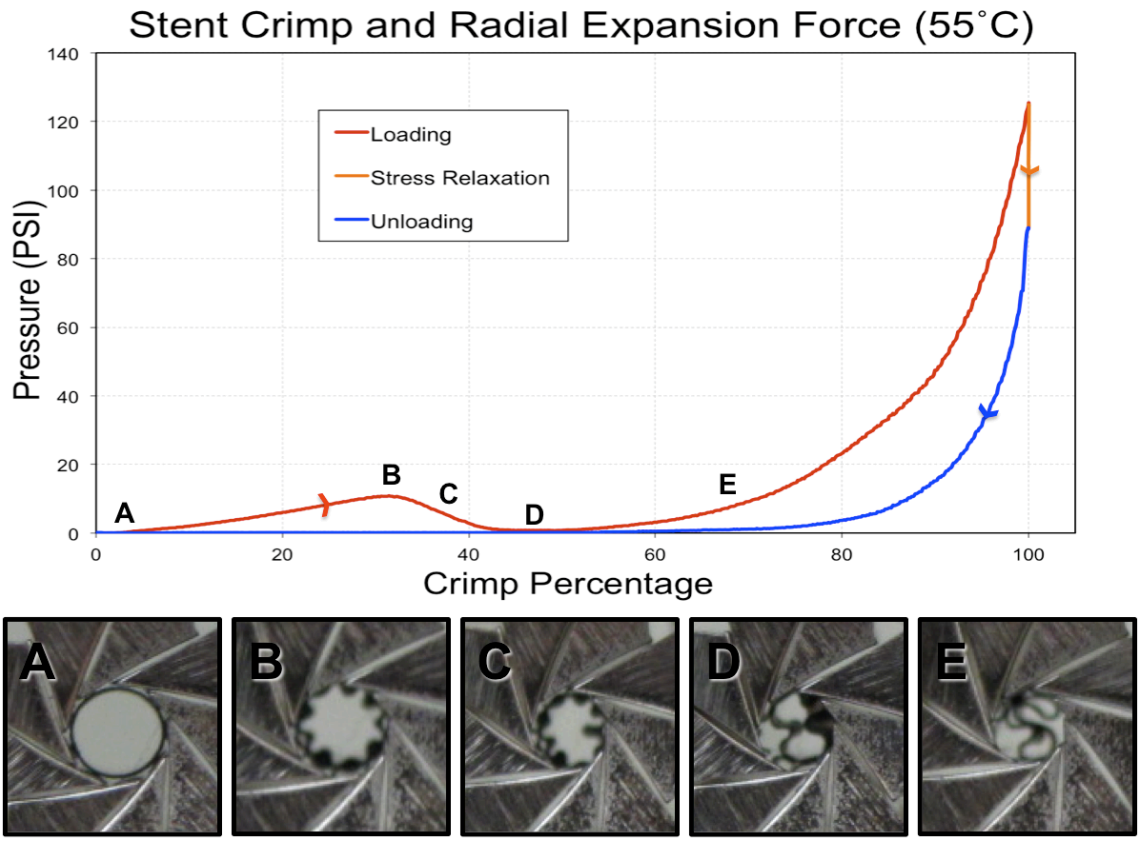

Figure 14 Breakdown of stent crimping and unloading behavior. Labeled regions of the curve match the corresponding crimp picture below. Pressure increases during star formation and drops after material buckling. Pressure starts to increase again when the stent doubles over multiple times.

The top portion of the figure shows stent mechanical behavior, while the labeled pictures below show tube crimping profiles to give a representative view of the device geometry. The red portion of the curve indicates material loading during the crimp. There is an increase in stress from points A to B as the circular stent cross section takes on a nine

pointed star pattern. At point C, there is a decrease in stress as one of the star points buckles into the interior. There is a complete reduction in stress due to extensive buckling at point D. It is important to note that this zero-stress portion typically occurs between 40-55 crimp percent. These crimp percentage values will show interesting behavior during device recovery, which is to be presented in future sections. This buckling behavior, which does not occur in a completely repeatable manner, can be problematic for predicting the stress and geometry of the material during crimping. At point E the stress begins to rise again until the ultimate crimping pressure is reached. Crimping pressure is analogous to collapse pressure, but not the same. This crimping pressure is useful to understand the device fabrication process, but the mechanics of the crimping station are vastly different from a collapsing blood vessel. The compression station value is a pressure in that it is a force per unit area, but it is not the same as a pressure gradient between the interior and exterior of a compliant tube. A collapsing vessel flattens when exposed to an external pressure, rather than folding into an organized crimp. Thus, this crimping pressure cannot be referred to as the collapse pressure, which is a more physiologically relevant value. The orange portion of the curve shows stress relaxation when the crimp is held constant.

Figure 15 is the exact same loading cycle as figure 14, but shown as a function of time. The orange stress relaxation portion is easier to see in this time dependent figure. This stress relaxation is due to the visco-elastic nature of the polymer and is likely dependent on the crimping rate. The blue portions of each figure show the force exerted by the

material while the compression station is opened back to the original diameter. According to this curve, there is a negligible amount of force being exerted by the material below ~70 crimp percent. However, additional tests will prove this to be inaccurate. It is suspected that the crimping station is opening too fast for the sample to recover to its maximum force at 55˚C.

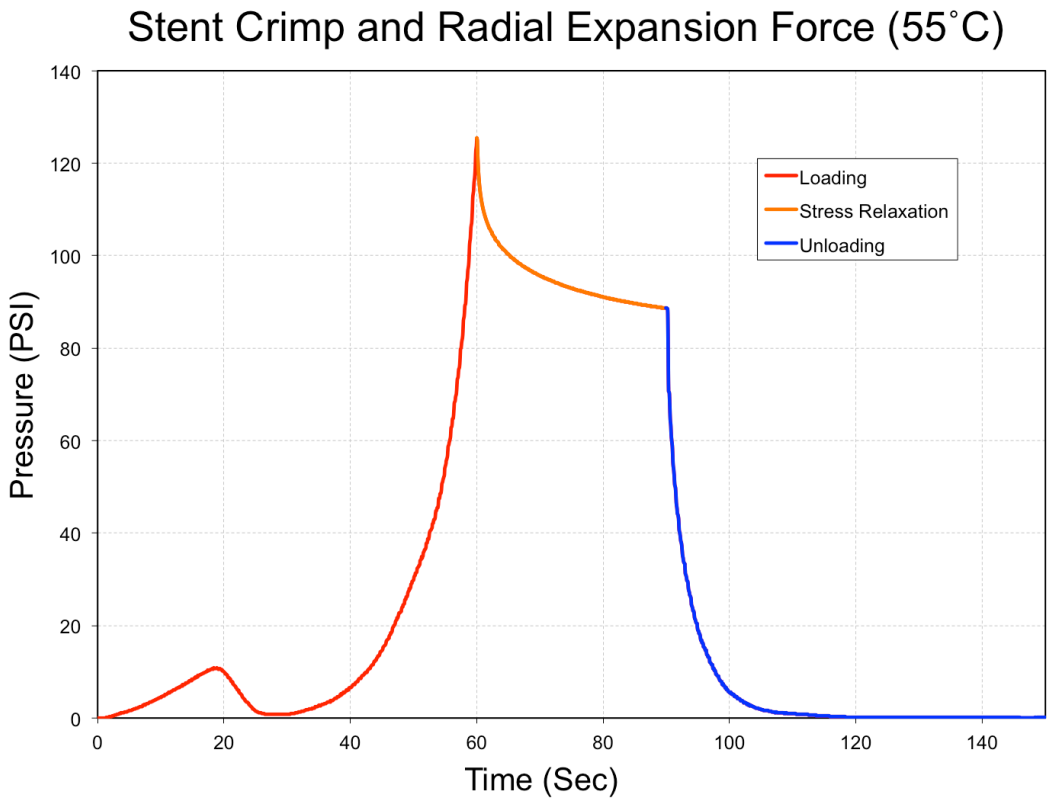

Figure 15 Stress relaxation is more apparent in this time dependent curve. This is the same data set as the curve breakdown in figure 14.

Figure 16 shows a comparative increase in crimping pressure and recovery pressure with increasing stent wall thickness. Sufficient wall thickness is important to have enough

radial force to keep the vessel open, but stent struts that are too thick can impede blood flow and negatively disrupt the flow profile.

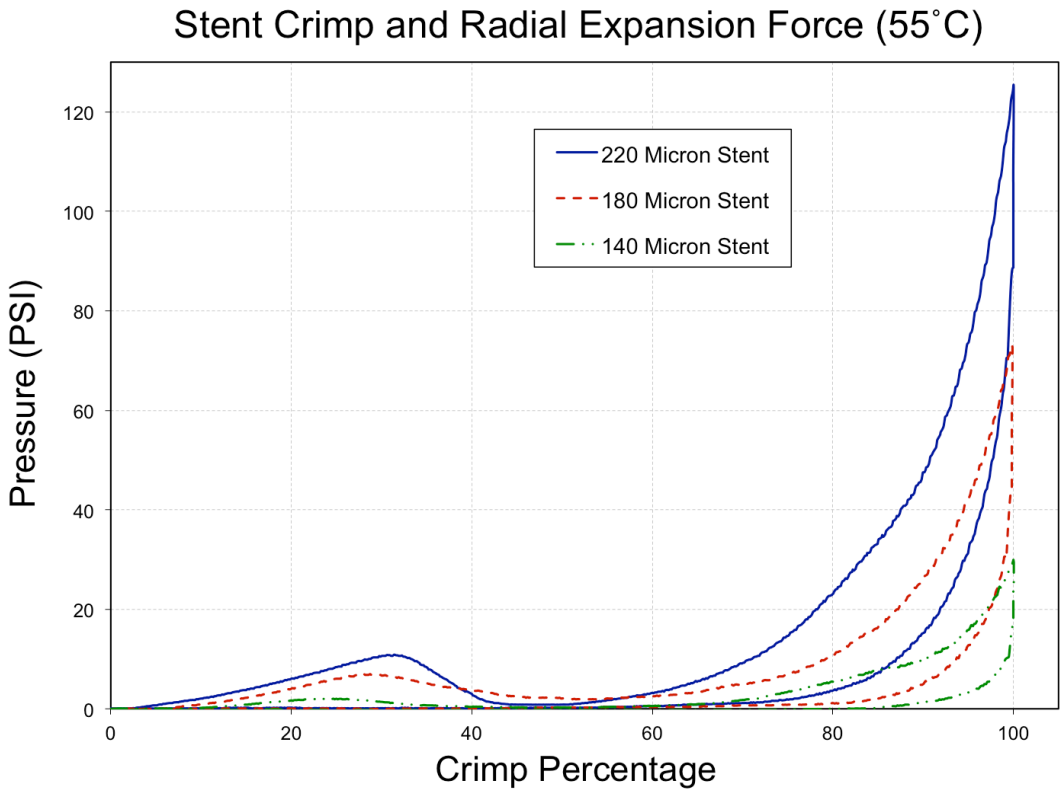

Figure 16 Comparison of crimping force and recovery behavior of stents with increasing wall thickness. There is a clear trend in increasing crimping pressure with increasing wall thickness.

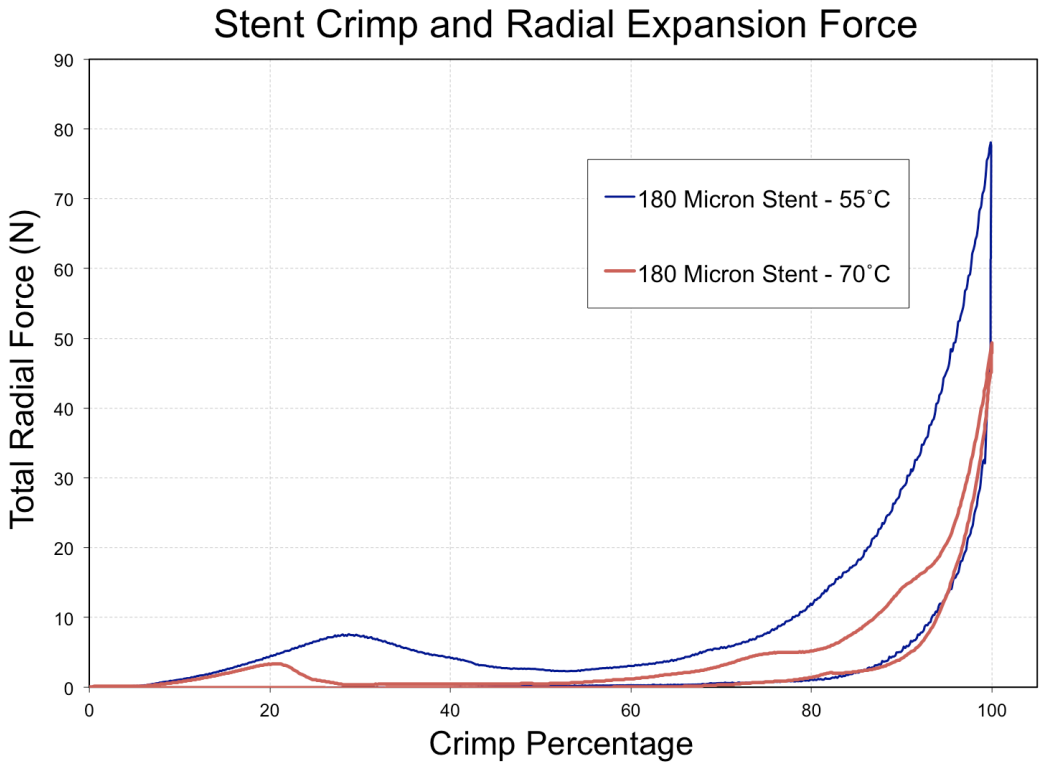

Figure 17 Comparison of stent crimping at T = T_g and T > T_g. Pressure values are lower at higher temperature because the material is in its rubbery state. The less homogeneous shape of the high temperature curve is being attributed to material failure during the crimping process.

Figure 17 shows crimping profiles of 180 micron thick stents at T_g (55˚C) and 15 degrees above T_g when the material is within the rubbery plateau. As expected, the higher temperature curve exhibited lower radial forces due to the material being more rubbery. Additionally, all stents that were crimped at 70˚C showed creasing and breaking after crimping and subsequent recovery. Thus, these devices should not be crimped above T_g because the material may not be tough enough to withstand the crimping strains. The 70˚C curve is much less smooth when compared to the 55˚C curve, and it is proposed that the bumps are associated with material failure during the crimping process at higher temperatures.

Constrained radial recovery

Figure 18 shows the behavior of polymer tubes when deployed into a fixed diameter environment, similar to deploying within an occluded vessel. These rings are idealizations of the overall stent, representing the rings within the stent design. These tests quantify how much pressure the device can exert as a function of temperature.

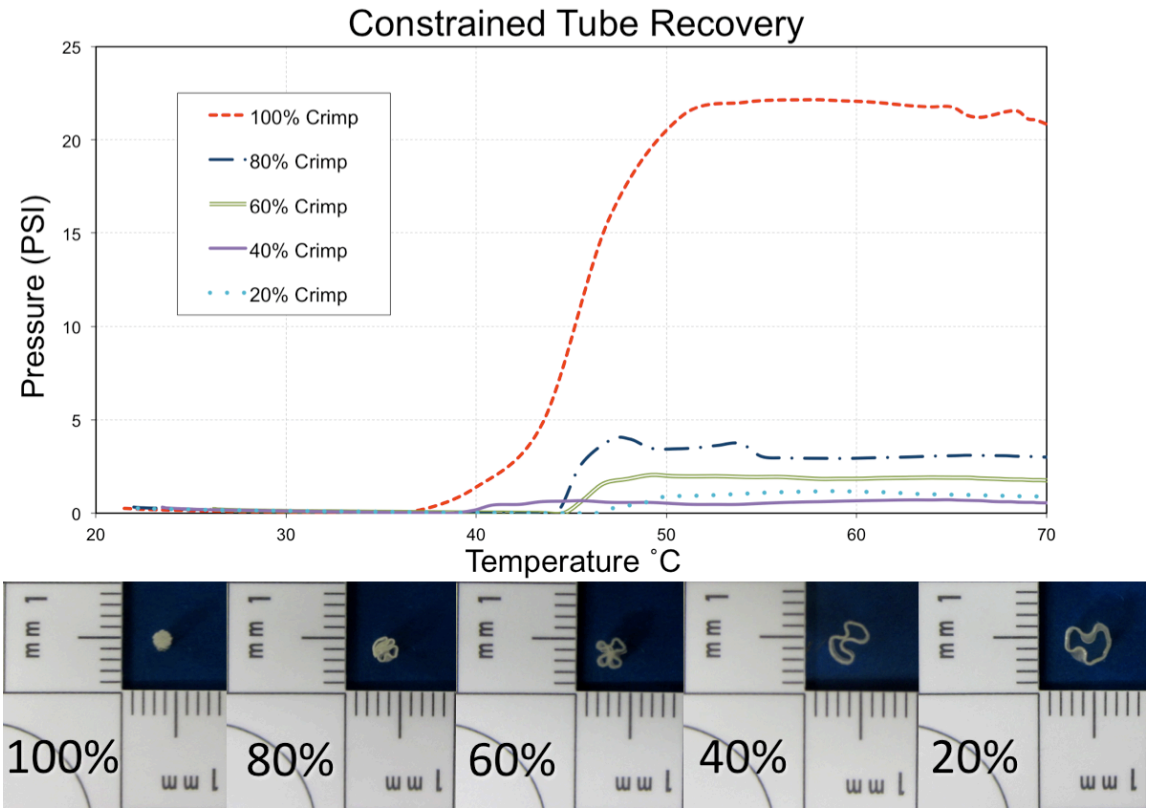

Figure 18 Constrained tube pressure recovery as a function of temperature. The resulting geometries for each crimp percentage are depicted below the curve. The 40% curve does not follow the expected trend, highlighting the fact that these recovery pressures are highly dependent on the crimp geometry.

The data from figure 18 is more representative of device in vivo recovery than that presented in figures 14-17 because deployment in a vessel is a constrained recovery

environment. These curves have a wavy appearance before reaching an eventual plateau due to unfolding and sudden changes in the recovering geometry until a stable shape is reached. There is a trend with decreasing recovery pressure with decreasing crimp%. However, the 40 crimp% does not follow this trend because it registers pressures below the 20 crimp%. This behavior can be linked back to the crimping behavior explained in figure 14. The crimp percentages associated with part D of the curve show that no stress is exerted radially due to buckling. These same geometry conditions seem to be contributing to the constrained recovery force. A stress cannot be recovered unless it is "programmed" into the material. This behavior will need to be considered in the clinical application of this device. It will be important to have a way to verify that the device deploys beyond a 40 crimping percent in vivo. Also, the pressures exerted by the device are not sufficient enough to clear an atherosclerotic plaque, so it will most likely need to be deployed in conjunction with a balloon angioplasty. Although this complicates the delivery procedure, low device pressures at full expansion will minimize the force exerted on the diseased vessel wall. This is an advantage because these tissues can be mechanically compromised and prone to rupture.

Future work

Computational models can be powerful tools for streamlining the design process of medical devices. Finite element analysis is employed in the design of traditional nitinol stents[28, 29], and a constitutive model of nitinol has been employed to optimize the design of a braided stent[30]. However, constitutive modeling of SMPs is much less prevalent in

the design of stents. A constitutive model of these shape memory materials implemented in 3D can be a powerful tool for optimizing medical devices, but it is important to validate the developed model with multi-axial experimental data. Even if the constitutive model is calibrated according to one-dimensional tensile data, it is still important to get physical multidimensional characterization to validate the efficacy of the full computational model. Finite element analysis has been performed on a shape memory polymer polyurethane stent prototype[31], but the results of the model were not validated with experimental data.

The radial crimping and expansion data from this thesis could be used for an initial validation of a multidimensional computational model of shape memory polymers. The constrained tube recovery tests will be ideal for validation purposes because they involve a simplified geometry that enables straightforward modeling. However, the complex geometric considerations involved with device crimping and uncrimping will complicate the model beyond characterizing the material shape memory behavior. Once the constitutive model is validated, it can be used to simulate and optimize a more complex stent design and other medical devices.

CHAPTER IV

SUMMARY AND CONCLUSIONS

This study expanded on the clinical efficacy of a previously proposed stent design by quantifying the longitudinal flexibility, shape memory abilities, gel fraction, and expansion pressures of the device. With longitudinal stiffness values comparable to flexible devices available on the market, these devices show promise in neurovascular applications requiring increased compliance to deploy in tortuous vessels. The excellent shape memory of these materials allows the device to deploy in one second. This rapid deployment allows for controlled device delivery, and reduces the amount of heat introduced into the vascular environment. Although the expansion pressures produced by these devices are not sufficient to clear an atherosclerotic plaque, low expansion pressures reduce the risk of rupturing a mechanically compromised diseased vessel wall.

The thermo-mechanical characterization of these devices, such as recovery pressures and optimal crimping techniques, provides data relevant to the clinical implementation of the device design. This data could also be used as an initial validation of a thermo-mechanical computational model. An accurate model would be helpful in the design and optimization of novel SMP biomedical devices including stents and thrombectomy devices. However, this data is not detailed enough to stand alone as the computational model validation. The unpredictable geometric changes during the crimping and

uncrimping process have shown that this device is not the best candidate for validating an intensive computational model.

Although this polymer system currently does not have all of the properties desirable of an optimized stent, it provides a solid platform for development of a fully functional device. The proposed composition displays mechanical properties desirable for stent applications. Future improvements for this polymer system include making it biodegradable, increasing the gel fraction to reduce potentially leachable material, and making it radio-opaque. It will also be necessary to quantify the biocompatibility of these polymers.

REFERENCES

1. Baer, G.; Wilson, T. S.; Matthews, D. L.; Maitland, D. J. J Appl Polym Sci 2007, 103, 3882.

2. Gall, K.; Yakacki, C. M.; Liu, Y.; Shandas, R.; Willett, N.; Anseth, K. S. J Biomed Mater Res A 2005, 73, 339.

3. Small Iv, W.; Wilson, T.; Benett, W.; Loge, J.; Maitland, D. Opt Express 2005, 13, 8204.

4. Ajili, S. H.; Ebrahimi, N. G.; Soleimani, M. Acta Biomater 2009, 5, 1519.

5. Baer, G. M.; Small, W., IV; Wilson, T. S.; Benett, W. J.; Matthews, D. L.; Hartman, J.; Maitland, D. J. Biomed Eng Online 2007, 6, 43.

6. Wache, H. M.; Tartakowska, D. J.; Hentrich, A.; Wagner, M. H. J Mater Sci Mater Med 2003, 14, 109.

7. Yakacki, C. M.; Shandas, R.; Lanning, C.; Rech, B.; Eckstein, A.; Gall, K. Biomaterials 2007, 28, 2255.

8. Roger, V. L.; Go, A. S.; Lloyd-Jones, D. M.; Adams, R. J.; Berry, J. D.; Brown, T. M.; Carnethon, M. R.; Dai, S.; de Simone, G.; Ford, E. S.; Fox, C. S.; Fullerton, H. J.; Gillespie, C.; Greenlund, K. J.; Hailpern, S. M.; Heit, J. A.; Ho, P. M.; Howard, V. J.; Kissela, B. M.; Kittner, S. J.; Lackland, D. T.; Lichtman, J. H.; Lisabeth, L. D.; Makuc, D. M.; Marcus, G. M.; Marelli, A.; Matchar, D. B.; McDermott, M. M.; Meigs, J. B.; Moy, C. S.; Mozaffarian, D.; Mussolino, M. E.; Nichol, G.; Paynter, N. P.; Rosamond, W. D.; Sorlie, P. D.; Stafford, R. S.; Turan, T. N.; Turner, M. B.; Wong, N. D.; Wylie-Rosett, J.; American Heart Association Statistics Committee and Stroke Statistics Subcommittee. Circulation 2011, 123, e18.

9. Higashida, R. T.; Meyers, P. M. Neuroradiology 2006, 48, 367.

10. Garg, S.; Serruys, P. W. J Am Coll Cardiol 2010, 56, S43.

11. Konig, A.; Schiele, T. M.; Rieber, J.; Theisen, K.; Mudra, H.; Klauss, V. Z Kardiol 2002, 91 Suppl 3, 98.

12. Waksman, R. Catheter Cardiovasc Interv 2007, 70, 407.

13. Finn, A. V.; Nakazawa, G.; Joner, M.; Kolodgie, F. D.; Mont, E. K.; Gold, H. K.; Virmani, R. Arterioscler Thromb Vasc Biol 2007, 27, 1500.

14. Amano, Y.; Ishihara, M.; Hayashi, H.; Gemma, K.; Kawamata, H.; Amano, M.; Kumazaki, T. Clin Imaging 1999, 23, 85.

15. Klemm, T.; Duda, S.; Machann, J.; Seekamp-Rahn, K.; Schnieder, L.; Claussen, C. D.; Schick, F. J Magn Reson Imaging 2000, 12, 606.

16. Tamai, H.; Igaki, K.; Kyo, E.; Kosuga, K.; Kawashima, A.; Matsui, S.; Komori, H.; Tsuji, T.; Motohara, S.; Uehata, H. Circulation 2000, 102, 399.

17. Tanimoto, S.; Serruys, P. W.; Thuesen, L.; Dudek, D.; de Bruyne, B.; Chevalier, B.; Ormiston, J. A. Catheter Cardiovasc Interv 2007, 70, 515.

18. Baer, G. M.; Wilson, T. S.; Small, W.,4th; Hartman, J.; Benett, W. J.; Matthews, D. L.; Maitland, D. J. J Biomed Mater Res B Appl Biomater 2009, 90, 421.

19. Rolland, P. H.; Mekkaoui, C.; Vidal, V.; Berry, J. L.; Moore, J. E.; Moreno, M.; Amabile, P.; Bartoli, J. M. Eur J Vasc Endovasc Surg 2004, 28, 431.

20. De Jong, W. H.; Eelco Bergsma, J.; Robinson, J. E.; Bos, R. R. M. Biomaterials 2005, 26, 1781.

21. Rodriguez, J. N.; Yu, Y. J.; Miller, M. W.; Wilson, T. S.; Hartman, J.; Clubb, F. J.; Gentry, B.; Maitland, D. J. Ann Biomed Eng 2011.

22. Chen, M. C.; Tsai, H. W.; Chang, Y.; Lai, W. Y.; Mi, F. L.; Liu, C. T.; Wong, H. S.; Sung, H. W. Biomacromolecules 2007, 8, 2774.

23. Buckley, P. R.; McKinley, G. H.; Wilson, T. S.; Small, W.; Benett, W. J.; Bearinger, J. P.; McElfresh, M. W.; Maitland, D. J. IEEE Trans Biomed Eng 2006, 53, 2075.

24. Ormiston, J. A.; Dixon, S. R.; Webster, M. W.; Ruygrok, P. N.; Stewart, J. T.; Minchington, I.; West, T. Catheter Cardiovasc Interv 2000, 50, 120.

25. Volk, B.L.; Lagoudas D.C.; Maitland, D.J. Smart Mater Struct 2011, 20, 094004.

26. ASTM F 2606-08. "Standard Guide for Three-Point Bending of Balloon Expanding Vascular Stents and Stent Systems." ASTM International, 2008. West Conshohocken, PA 19428.

27. Park, J.; Ye, Q.; Topp, E. M.; Lee, C. H.; Kostoryz, E. L.; Misra, A.; Spencer, P. Journal of Biomedical Materials Research Part B: Applied Biomaterials 2009, 91B, 61.

28. Donnelly, E. W.; Bruzzi, M. S.; Connolley, T.; McHugh, P. E. Comput Methods Biomech Biomed Engin 2007, 10, 103.

29. Theriault, P.; Terriault, P.; Brailovski, V.; Gallo, R. J Biomech 2006, 39, 2837.

30. Kim, J. H.; Kang, T. J.; Yu, W. R. J Biomech 2008, 41, 3202.

31. Kim, J. H.; Kang, T. J.; Yu, W. R. J Biomech 2010, 43, 632.

CONTACT INFORMATION

Name:	Landon D. Nash
Professional Address:	c/o Dr. Duncan Maitland Department of Biomedical Engineering 5045 Emerging Technologies Building MS 3120 Texas A&M University College Station, TX 77843
Email Address:	nashlandon@gmail.com
Education:	B.S., Biomedical Engineering, Texas A&M University, May 2013 Summa Cum Laude Undergraduate Research Scholar (May 2012) Alpha Eta Mu Beta